

Vorticity Determines the Force on Bodies Immersed in Active Fluids

Thomas Speck and Ashreya Jayaram

Institut für Physik, Johannes Gutenberg-Universität Mainz, Staudingerweg 7-9, 55128 Mainz, Germany

When immersed into a fluid of active Brownian particles, passive bodies might start to undergo linear or angular directed motion depending on their shape. Here we exploit the divergence theorem to relate the forces responsible for this motion to the density and current induced by—but far away from—the body. In general, the force is composed of two contributions: due to the strength of the dipolar field component and due to particles leaving the boundary, generating a non-vanishing vorticity of the polarization. We derive and numerically corroborate results for periodic systems, which are fundamentally different from unbounded systems with forces that scale with the area of the system. We demonstrate that vorticity is localized close to the body and to points at which the local curvature changes, enabling the rational design of particle shapes with desired propulsion properties.

The defining feature of mesoscopic active matter [1, 2] is the persistent Brownian motion of its constituents, *i.e.*, particles have a tendency to continue moving in the direction of previous displacements. The resulting motion is characterized as self-propulsion or, in a solvent, “microswimming”. In contrast to passive diffusion, such an orientational persistence breaks detailed balance and thus requires steady dissipation. Some of the dissipated heat can be reclaimed as useful work and strategies on how to turn active matter into living and synthetic micro-engines have been proposed recently [3, 4]. Designing and optimizing such engines requires a comprehensive theoretical understanding of the forces generated in active fluids and suspensions [5].

Asymmetry plays a crucial role for self-propulsion. Spherical colloidal particles can break their symmetry through different surface properties, most often in the form of Janus particles with two distinct hemispheres, one active and the other one inert [6, 7]. Active but uniform particles might remain inert individually, but mixed with passive particles they aggregate into clusters that show directed linear and angular motion depending on the cluster’s symmetry [8–10]. To be distinguished from these modular microswimmers [11] are passive bodies placed into a suspension of, typically much smaller, active particles. Due to their directed motion, these particles get trapped and aggregate at the body’s surface [12], which induces a non-uniform density profile that is accompanied by an active stress and collective forces [5]. That passive but asymmetrically shaped bodies are subjected to directional forces has been demonstrated experimentally using microgears immersed into a bacterial bath [3, 13, 14], which undergo forward rotation on average. Related phenomena are current rectification [15–18] and trapping [19, 20] of active particles due to single obstacles or arrays of fixed obstacles. Trapping and aggregation also occurs on walls confining an active fluid, giving rise to the notion of active (or swim) pressure, a phenomenon that has been under intense scrutiny [21–31].

Forces on (rigid) bodies immersed in active fluids have

been studied numerically [32–37]. Analytical studies have followed two strategies: While Yan and Brady focus on the density distribution within the interaction layer of trapped active particles close to the body [38], Baek *et al.* relate the force to a dipolar algebraic decay of density and current in the far-field regime away from the body [39, 40]. Here we connect both approaches through the divergence theorem, which relates the force due to a complicated density distribution in the interaction layer to the—potentially much simpler—solution for a free fluid far away from the body. We show that the force has two contributions, one from the far-field dipole and one from the vorticity of the polarization diffusing out of the interaction layer. While bodies in unbounded systems indeed appear as dipoles from a distance, this changes fundamentally in finite systems, where now the vorticity cancels the long-range dipolar field and sustains the force on the immersed body.

We study a “dry” fluid of non-interacting active particles moving with constant speed v_0 in two dimensions. The joint probability $\psi(\mathbf{r}, \varphi; t)$ obeys the evolution equation

$$\partial_t \psi = -\nabla \cdot [v_0 \mathbf{e} \psi + \mu_0 \mathbf{F} \psi - D_0 \nabla \psi] + \frac{1}{\tau_r} \frac{\partial^2 \psi}{\partial \varphi^2}, \quad (1)$$

where $\mathbf{e} \equiv (\cos \varphi, \sin \varphi)^T$ is the unit orientation that undergoes rotational diffusion with correlation time τ_r . We assume that the translational diffusion coefficient $D_0 = k_B T \mu_0$ is related to the bare mobility μ_0 through the temperature T (with Boltzmann’s constant k_B), which could be an effective temperature. The force $\mathbf{F}(\mathbf{r})$ onto the active particles stems from walls and immersed objects and does not depend on the orientation φ .

We follow the standard route [5, 41] and consider the hierarchy of moments with respect to the orientation φ . Integrating Eq. (1) over φ leads to the continuity equation $\partial_t \rho + \nabla \cdot \mathbf{j} = 0$ with density $\rho(\mathbf{r}, t) \equiv \int_0^{2\pi} d\varphi \psi$ and particle current

$$\mathbf{j} = v_0 \mathbf{p} + \mu_0 \mathbf{F} \rho - D_0 \nabla \rho. \quad (2)$$

Here the polarization $\mathbf{p}(\mathbf{r}, t) \equiv \int_0^{2\pi} d\varphi \mathbf{e}\psi$ enters. In the following, we drop the time dependence and consider the steady state with $\nabla \cdot \mathbf{j} = 0$ everywhere. Multiplying Eq. (1) by \mathbf{e} followed again by integration over φ now yields

$$0 = -\nabla \cdot \left[\frac{v_0}{2} \rho \mathbf{1} + v_0 \mathbf{Q} + \mu_0 \mathbf{F} \mathbf{p} - D_0 \nabla \mathbf{p} \right] - \frac{1}{\tau_r} \mathbf{p}, \quad (3)$$

where \mathbf{Q} is the nematic tensor. To close the hierarchy, this tensor can be approximated as $\mathbf{Q} \approx -(v_0 \tau_r / 16) (\nabla \mathbf{p})^{ST}$ [42]. For the direct product, we write $(\mathbf{F} \mathbf{p})_{ij} = F_i p_j$ in cartesian coordinates and we employ the Einstein sum convention over repeated indices. The symmetric and traceless derivative reads $(\nabla \mathbf{p})_{ij}^{ST} = \partial_i p_j + \partial_j p_i - (\nabla \cdot \mathbf{p}) \delta_{ij}$. Through Eq. (3), the polarization $v_0 \mathbf{p} = \mu_0 \nabla \cdot \boldsymbol{\sigma}_A$ can be related to the divergence of a tensor

$$\boldsymbol{\sigma}_A = -v_0 \tau_r \left[\frac{v_0}{2\mu_0} \rho \mathbf{1} + \frac{v_0}{\mu_0} \mathbf{Q} + \mathbf{F} \mathbf{p} - k_B T (\nabla \mathbf{p})^{ST} \right] \quad (4)$$

that can be interpreted as an active stress. Note that we symmetrize the last term, which does not change the divergence. Replacing $v_0 \mathbf{p}$ in Eq. (2), we thus find the balance equation

$$\nabla \cdot \boldsymbol{\sigma} + \mathbf{F} \rho = \mathbf{j} / \mu_0 \quad (5)$$

with total stress tensor $\boldsymbol{\sigma} = -k_B T \rho \mathbf{1} + \boldsymbol{\sigma}_A$. A uniform fluid has constant density $\rho = \rho_\infty$ and vanishing polarization, $\mathbf{p} = 0$, for which the stress is isotropic.

We consider immersed objects (and possibly walls) with a finite interaction range, *i.e.*, beyond a certain (microscopic) distance the force $\mathbf{F} = 0$ vanishes and the active particles away from walls and bodies move freely. This defines disjoint regions, a “free” region in which $\mathbf{F} = 0$ bounded by several regions with $\mathbf{F} \neq 0$ corresponding to each body within which the density ρ of active particles declines sharply, defining a thin interaction layer at the surface of bodies. Due to their persistent motion, active particles are trapped at bodies and accumulate within the interaction layer generating an inhomogeneous density $\rho(\mathbf{r})$ also in the free region. More importantly, such an inhomogeneous density is accompanied by a non-vanishing polarization and, consequently, a non-isotropic active stress Eq. (4).

The force \mathbf{F}_1 on a single body is minus the total force exerted on the fluid. One route is to estimate the density within the interaction layer [30, 43]. Here we follow a different strategy and, together with Eq. (5), exploit the divergence theorem to rewrite

$$\mathbf{F}_1 = - \int_A d^2 \mathbf{r} \mathbf{F} \rho = \oint_{\partial A} dl \left[\mathbf{n} \cdot \boldsymbol{\sigma} - \frac{1}{\mu_0} (\mathbf{n} \cdot \mathbf{j}) \mathbf{r} \right] \quad (6)$$

as a line integral along the closed curve ∂A bounding the integration area A (with normal vector \mathbf{n} pointing

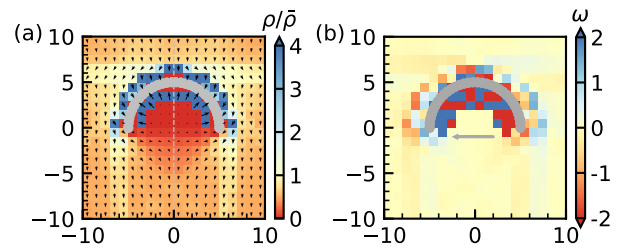


FIG. 1. Line-symmetric boomerang-shaped body. (a) Reduced density $\rho/\bar{\rho}$ (heat map) and polarization \mathbf{p} (arrows) of active particles (with global density $\bar{\rho} = N/L^2 = 1.2$ and speed $v_0 = 80$). Shown is a close-up of the body, the total system is larger. The length of arrows is calculated as the logarithm of the local polarization magnitude. (b) Vorticity map ω . Note the antisymmetric $\omega(-x, y) = -\omega(x, y)$ yielding a vanishing monopole moment $Q = 0$ and a non-vanishing dipole moment $\mathbf{P} = P \mathbf{e}_x$ (arrow).

outwards). For the second term we have used the identity $j_k = \partial_i (j_i x_k)$ with $\nabla \cdot \mathbf{j} = \partial_i j_i = 0$. The integration area A completely covers the body but is otherwise arbitrary (since $\mathbf{F} = 0$ in the free region). The curve ∂A lies completely within the force-free region, which reduces the determination of the local stress and current to a linear and homogeneous boundary-value problem away from the body.

To demonstrate the emergence of orientational order, we perform numerical simulations of N non-interacting active particles surrounding a “boomerang”-shaped body (semicircle with radius R) shown in Fig. 1. We employ a square box with edge length L and periodic boundary conditions (Supplemental Information [44]). The shape is constructed as overlapping points repelling the active particles through the finite-range Weeks-Chandler-Andersen potential. Throughout, numerical results are presented in units of the potential length scale a and time a^2/D_0 . We calculate the local density and polarization on a regular grid plotted in Fig. 1(a). We observe the aggregation of active particles directly at the surface of the body accompanied by a non-vanishing polarization due to the trapping of particles. But even away from the body there is a polarization of the active fluid with a pattern that is reminiscent of flow around a body. We stress that there is no alignment between particle orientations and this ordering is entirely due to the different retention times of particles at the top and bottom side of the boomerang.

To obtain the force on the boomerang in an infinite system it is sufficient to consider the decay of density and current far away from the body thanks to Eq. (6). We again turn to Eq. (3), which after eliminating the polarization through $v_0 \mathbf{p} = D_0 \nabla \rho + \mathbf{j}$ [Eq. (2)] becomes

$$-D_0 (\nabla^2 - \xi^{-2}) \nabla \rho = (\nabla^2 - \ell^{-2}) \mathbf{j} \quad (7)$$

in the free region. Here we have introduced two length

scales,

$$\ell \equiv \sqrt{D_0 \tau_r} \left(1 + \frac{v_0^2 \tau_r}{16 D_0} \right)^{1/2} \quad (8)$$

and the decay length

$$\xi \equiv \ell \left(1 + \frac{v_0^2 \tau_r}{2 D_0} \right)^{-1/2} \leq \ell \quad (9)$$

with persistence length $v_0 \tau_r$ of the directed motion. Assuming a body shape that does not generate currents ($\mathbf{j} = 0$), we find $\nabla(\nabla^2 \rho - \rho/\xi^2) = 0$. To obtain the full density profile, this equation has to be solved for the densities prescribed at the boundaries of the free region. However, we can immediately infer that the excess density $\rho - \rho_\infty \sim e^{-r/\xi}$ decays exponentially far away from the body. Hence, we can push out the integration boundary ∂A in Eq. (6) to distances where the density is uniform and, consequently, the stress is isotropic and the force thus zero.

Taking the divergence of Eq. (7) yields for the density $(\nabla^2 - \xi^{-2})\nabla^2 \rho = 0$ with now $\nabla^2 \rho \sim e^{-r/\xi} \approx 0$ sufficiently far away from the body [38]. The far-field density profile is thus the solution of $\nabla^2 \rho^{\text{ff}} = 0$ with current

$$\mathbf{j}^{\text{ff}} = -D_{\text{eff}} \nabla \rho^{\text{ff}}, \quad D_{\text{eff}} \equiv D_0 (\ell/\xi)^2. \quad (10)$$

An alternative route is to assume that the polarization decays slowly (on lengths much larger than ℓ). In this limit, we can drop the second derivative in Eq. (3) to obtain $\mathbf{p}^{\text{ff}} \approx -\frac{1}{2} v_0 \tau_r \nabla \rho^{\text{ff}}$ and thus Eq. (10).

The determination of the far-field current and density thus reduces to a problem that is well known from magnetostatics (with “field” \mathbf{j} and scalar potential ρ). Let us consider the *vorticity*

$$\omega(\mathbf{r}) \equiv \nabla \times \mathbf{p} \equiv \varepsilon_{ij} \partial_i p_j = \partial_x p_y - \partial_y p_x \quad (11)$$

of the polarization, where ε_{ij} is the Levi-Civita symbol with entries $\varepsilon_{ii} = 0$, $\varepsilon_{12} = -\varepsilon_{21} = 1$. This vorticity has to be generated by the body, which is demonstrated for the boomerang in Fig. 1(b). We find that at the ends of the arc vorticity is largest with opposite signs. Taking the curl of Eq. (7), the left hand side vanishes and we obtain the Helmholtz equation $\nabla^2 \omega - \omega/\ell^2 = 0$ in the free region, corroborating the numerical observation that the vorticity decays fast (on the length ℓ) and is localized close to the body. It would be exactly zero for currents of the form Eq. (10) at variance with Fig. 1(b).

The first two moments of the vorticity are the total “charge” $Q \equiv \int d^2 \mathbf{r} \omega = \oint d\mathbf{l} \cdot \mathbf{p}$ and the dipole moment $\mathbf{P} \equiv \int d^2 \mathbf{r} \mathbf{r} \omega$. In an unbounded system $Q = 0$ (the boundary is at infinity) and there can be no angular current $\mathbf{j}_\theta \sim \mathbf{e}_\theta/r$. This should be intuitively clear given that rotational diffusion implies that without a density gradient the local polarization relaxes to zero, preventing

such a rigid-body-like rotation of the fluid. The dipole moment

$$\mathbf{P}(A) = \oint_{\partial A} d\mathbf{l} \left[(\mathbf{n} \times \mathbf{p}) \mathbf{r} - \frac{\mu_0}{v_0} \boldsymbol{\varepsilon} \cdot (\mathbf{n} \cdot \boldsymbol{\sigma}_A) \right] \quad (12)$$

can be expressed as a contour integral after performing an integration by parts and replacing $v_0 \mathbf{p} = \mu_0 \nabla \cdot \boldsymbol{\sigma}_A$ in the bulk term followed by the divergence theorem. Expanding the current $\mathbf{j}(\mathbf{r})$ expressed through the Biot-Savart law, the far-field solution is given by the dipole field

$$\mathbf{j}^{\text{ff}} = \frac{1}{2\pi} \left[\frac{2(\mathbf{m} \cdot \mathbf{r}) \mathbf{r}}{r^4} - \frac{\mathbf{m}}{r^2} \right], \quad \rho^{\text{ff}} = \rho_\infty + \frac{1}{D_{\text{eff}}} \frac{\mathbf{m} \cdot \mathbf{r}}{2\pi r^2} \quad (13)$$

with current dipole moment $\mathbf{m} \equiv v_0 \boldsymbol{\varepsilon} \cdot \mathbf{P} - \mu_0 \mathbf{F}_1$ (Supplemental Information [44]). It has two contributions, the first due to the vorticity of the polarization surrounding the body and the second due to the forces within the interaction layer, both contributing to $\Omega \equiv \nabla \times \mathbf{j}$. However, plugging the far-field solution Eq. (13) into Eq. (12) we find for an unbounded system $\mathbf{P}_{\text{umb}} = 0$ independent of A and $\mathbf{F}_1 = -\mathbf{m}/\mu_0$ in agreement with Ref. 39. The same result is obtained plugging Eq. (13) into Eq. (6) [44]. Note, however, that Fig. 1(b) demonstrates that the vorticity dipole moment \mathbf{P} does not vanish in the simulations, again indicating that the dipolar solution [Eq. (13)] is not applicable.

Computer simulations are necessarily performed in a finite simulation box employing periodic boundaries. Naively assuming a lattice of dipoles, within a shell of radii r sufficiently far from the body *and* boundary ($R \ll r \ll L$), to leading order the density is unmodified and given by the dipole Eq. (13) [44]. However, the numerical density shown in Fig. 2(a) computed for a system with $L/R = 14$ deviates strongly from this expected profile. The current streamlines, instead of bending back as

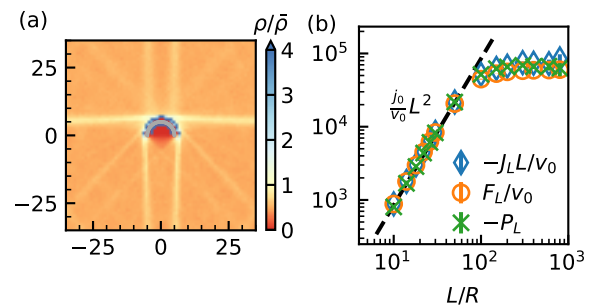


FIG. 2. Finite-size behavior in periodic systems. (a) Density profile ρ for the same parameters as Fig. 1 but showing the full system. Note the strong departure from a dipolar field with “streaks” connecting through the periodic boundaries. (b) Numerical current $-J_L L/v_0$, force F_L/v_0 , and vorticity dipole moment $-P_L$ as a function of box size L . All quantities agree and scale as L^2 for small system sizes (dashed line with $j_0/v_0 \simeq 0.34$) before crossing over to a constant value $-P_\infty$ beyond $L^* \simeq 50R$. Numerical data is shown for $v_0 = 160$.

for the dipole, now connect through the periodic boundaries. This results in a total current

$$J_L \equiv \int_{-L/2}^{L/2} dx j_y(x, y) < 0 \quad (14)$$

through a cross section spanning the system, which has to be independent of y since the divergence of the particle current is zero. As shown in Fig. 2(b), the current $J_L = j_0 L$ increases linearly for small cross sections L and decays as $J_L \sim 1/L$ for large L (the scaling is discussed in more detail in the Supplemental Information [44]).

In contrast to unbounded systems, from symmetry arguments alone we find that $\oint_{\partial A} dl \mathbf{n} \cdot \boldsymbol{\sigma} = 0$ in periodic systems, where the contour ∂A is the square bounding the simulation box (Supplemental Information [44]). As a corollary, the total polarization $\int d^2\mathbf{r} \mathbf{p} = (\mu_0/v_0) \oint dl \mathbf{n} \cdot \boldsymbol{\sigma}_A = 0$ also vanishes, which is confirmed by the simulations. Hence, the polarization in the free region and within the interaction layer compensate each other. The force on the body

$$\mathbf{F}_1 = -\frac{1}{\mu_0} \oint_{\partial A} dl (\mathbf{n} \cdot \mathbf{j}) \mathbf{r} = F_L \mathbf{e}_y \quad (15)$$

is now entirely determined by the size-dependent current with $F_L = -L J_L / \mu_0$ [44]. This relation is confirmed numerically in Fig. 2(b). In addition, we determine the vorticity dipole moment $\mathbf{P} = P_L \mathbf{e}_x$ through numerical integration of the vorticity field ω . Figure 2(b) shows that the numerical values $-P_L$ agree with the force $\mu_0 F_L / v_0$ as predicted theoretically from Eq. (12) with $v_0 P_L = j_0 L^2$ [44].

The origin of the force on an immersed body in a periodic system is thus fundamentally different from the unbounded system: The strength of the far-field dipole $\mathbf{m} = v_0 \boldsymbol{\varepsilon} \cdot \mathbf{P} - \mu_0 \mathbf{F}_1 = -(v_0 P_L + \mu_0 F_L) \mathbf{e}_y = 0$ vanishes and the idea of a dipole lattice is not applicable. The vorticity ω diffusing into the free region now determines the current and the force on the body. This force can become very large, scaling as $F_L \sim L^2$ before saturating beyond $L^* \sim \sqrt{\ell R}$ to a constant force $F_\infty \sim v_0^2$ that increases quadratically with the speed. This insight has practical ramifications for the design of engines and pumps as it implies an optimal spacing of obstacles with separation L^* that maximizes the current and the force per obstacle. Moreover, it implies that inclusions cannot be modeled as dipoles in computer simulations.

Next, we perform simulations of the shape shown in Fig. 3, which consists of two semicircles cut and displaced along the x -axis. In agreement with its symmetry (no line symmetry, C_2 -symmetric), we measure no linear force $\mathbf{F}_1 = 0$ but a non-vanishing torque τ_1 . The torque can be written

$$\tau_1 = - \int_A d^2\mathbf{r} \mathbf{r} \times \mathbf{F} \rho = \int_A d^2\mathbf{r} \mathbf{r} \times [\nabla \cdot \boldsymbol{\sigma} - \mathbf{j} / \mu_0], \quad (16)$$

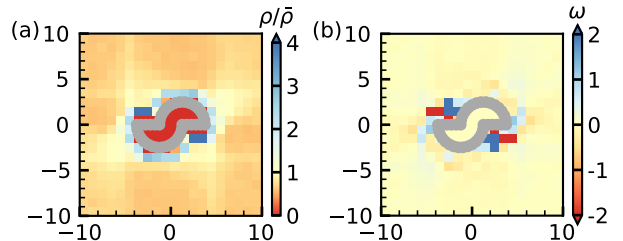


FIG. 3. C_2 -symmetric body. (a) Density profile and (b) vorticity map. Note the two dipoles forming at the shape's corners, which are responsible for the non-vanishing torque (while $Q = 0$).

where we have inserted the force balance Eq. (5). Again, we have an integration area A that has to cover the body but is otherwise arbitrary. It is straightforward but somewhat tedious to rewrite this expression so that it only contains the current (Supplemental Information [44]). Inserting the current multipole expansion, we find $\tau_1 \propto v_0 Q$. But also in a periodic system $Q = 0$ since the polarization on the boundary ∂A has to obey the periodic boundary conditions so that opposite edges cancel in the line integral $Q = \oint_{\partial A} dl \cdot \mathbf{p} = 0$.

The fact that $Q = 0$ seems to contradict the non-vanishing torque that we measure in the simulations. Inspecting the numerical vorticity map Fig. 3(b), we find indeed $Q = 0$ and also $\mathbf{P} = 0$. A closer look, however, reveals that now two local dipoles are present at the left and right “overhangs” of the shape with $\mathbf{P}_1 + \mathbf{P}_2 = 0$. In an unbounded system, decomposing the far-field current field into the contributions of dipoles at \mathbf{r}_n each with moment \mathbf{m}_n , $\mathbf{j}(\mathbf{r}) = \sum_n \mathbf{j}_n^{\text{ff}}(\mathbf{r} - \mathbf{r}_n)$, we find for the torque

$$\tau_1 = -\frac{1}{\mu_0} \int_A d^2\mathbf{r} \sum_n (\mathbf{r}_n + \mathbf{r}) \times \mathbf{j}_n^{\text{ff}}(\mathbf{r}) = \sum_n \mathbf{r}_n \times \mathbf{F}_n \quad (17)$$

using that $\int_A d^2\mathbf{r} \mathbf{r} \times \mathbf{j}_n^{\text{ff}} \sim Q_n = 0$, and \mathbf{F}_n is the force of dipole n with dipole moment \mathbf{m}_n . In finite systems, from the simulations we again find a quadratic scaling $\tau_1 \sim v_0 L^2$ with system size $L < L^*$ [44].

Figure 4 shows three shapes plotting the vorticity along the perimeter of each shape just outside the interaction layer. All shapes exhibit the same behavior: the vorticity ω is strongly localized close to points where the local curvature changes and is zero elsewhere. At these points local dipoles \mathbf{P}_n emerge, which determine whether the body experiences a linear force $\mathbf{F}_1 = (v_0/\mu_0) \sum_n \boldsymbol{\varepsilon} \cdot \mathbf{P}_n$, a torque $\tau_1 = -(v_0/\mu_0) \sum_n \mathbf{r}_n \cdot \mathbf{P}_n$, or both. This insight can be used to design shapes with the desired behavior.

To conclude, bodies immersed in an active fluid can induce currents depending on their shape, which act back on the body and cause linear and angular propulsion. The analogy of the underlying equation (7) in an unbounded force-free region is with magnetostatics (not electrostatics), whereby the field is generated by a steady

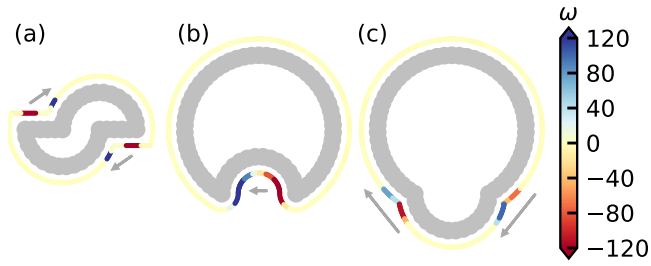


FIG. 4. Vorticity ω along the perimeter of three shapes: (a) the shape from Fig. 3, (b) a lune (subtracting a smaller disc) and (c) a bud (union with smaller disc). The vorticity is zero almost everywhere and localized to regions close to changes of the local curvature. Arrows indicate the local dipoles \mathbf{P}_n , which are oriented oppositely to the orientation of the perimeter.

“electric” current density $\Omega \mathbf{e}_z$ perpendicular to the plane of motion. While the force in an unbounded system is determined by the dipole contribution alone, passive inclusions are *not* force dipoles and the analogy breaks down for periodic arrays and periodic boundary conditions. Now the force is sustained by the polarization vorticity leaving the interaction layer and enables giant forces and torques.

Here we have studied several simple shapes with symmetries causing either linear or angular propulsion. Our results can be tested in experiments, *e.g.* in periodic arrays of rotors driven by bacteria [3]. Directed forces might be harvested for the self-assembly of passive bodies through active suspensions. An intriguing question concerns the optimal shape that maximizes the vorticity dipole moment \mathbf{P} . Refs. 19, 20 study the trapping of active particles in a wedge as a function of the opening angle. For our purposes we require a large accumulation together with a large exit current, which seems to be the case for intermediate angles $\sim \pi/2$ but needs to be investigated more carefully in future work.

We acknowledge funding by the Deutsche Forschungsgemeinschaft (DFG) within collaborative research center TRR 146 (Grant No. 404840447) and the priority program SPP 1726 (Grant No. 254473714). Computations have been performed on the supercomputer MOGON II.

[1] G. Gompper, R. G. Winkler, T. Speck, A. Solon, C. Nardini, F. Peruani, H. Löwen, R. Golestanian, U. B. Kaupp, L. Alvarez, T. Kioerboe, E. Lauga, W. Poon, A. D. Simone, F. Cichos, A. Fischer, S. M. Landin, N. Soeker, R. Kapral, P. Gaspard, M. Ripoll, F. Sagues, J. Yeomans, A. Doostmohammadi, I. Aronson, C. Bechinger, H. Stark, C. Hemelrijk, F. Nedelec, T. Sarkar, T. Aryaksama, M. Lacroix, G. Duclos, V. Yashunsky, P. Silberzan, M. Arroyo, and S. Kale, “The 2020 motile active matter roadmap,” *J. Phys. Con-*

dens. Matter **32**, 193001 (2020).

[2] C. Bechinger, R. D. Leonardo, H. Löwen, C. Reichhardt, G. Volpe, and G. Volpe, “Active particles in complex and crowded environments,” *Rev. Mod. Phys.* **88**, 045006 (2016).

[3] G. Vizsnyiczai, G. Frangipane, C. Maggi, F. Saglimbeni, S. Bianchi, and R. D. Leonardo, “Light controlled 3d micromotors powered by bacteria,” *Nat. Commun.* **8** (2017), 10.1038/ncomms15974.

[4] P. Pietzonka, E. Fodor, C. Lohrmann, M. E. Cates, and U. Seifert, “Autonomous engines driven by active matter: Energetics and design principles,” *Phys. Rev. X* **9**, 041032 (2019).

[5] T. Speck, “Collective forces in scalar active matter,” *Soft Matter* **16**, 2652–2663 (2020).

[6] J. R. Howse, R. A. L. Jones, A. J. Ryan, T. Gough, R. Vafabakhsh, and R. Golestanian, “Self-motile colloidal particles: From directed propulsion to random walk,” *Phys. Rev. Lett.* **99**, 048102 (2007).

[7] R. Golestanian, T. B. Liverpool, and A. Ajdari, “Designing phoretic micro- and nano-swimmers,” *New J. Phys.* **9**, 126 (2007).

[8] R. Soto and R. Golestanian, “Self-assembly of catalytically active colloidal molecules: Tailoring activity through surface chemistry,” *Phys. Rev. Lett.* **112**, 068301 (2014).

[9] R. Niu, A. Fischer, T. Palberg, and T. Speck, “Dynamics of binary active clusters driven by ion-exchange particles,” *ACS Nano* **12**, 10932–10938 (2018).

[10] B. Liebchen, R. Niu, T. Palberg, and H. Löwen, “Unraveling modular microswimmers: From self-assembly to ion-exchange-driven motors,” *Phys. Rev. E* **98**, 052610 (2018).

[11] R. Niu and T. Palberg, “Modular approach to microswimming,” *Soft Matter* **14**, 7554–7568 (2018).

[12] Y. Fily, A. Baskaran, and M. F. Hagan, “Dynamics of self-propelled particles under strong confinement,” *Soft Matter* **10**, 5609–5617 (2014).

[13] R. Di Leonardo, L. Angelani, D. Dell’Arciprete, G. Ruocco, V. Iebba, S. Schippa, M. P. Conte, F. Mecarini, F. De Angelis, and E. Di Fabrizio, “Bacterial ratchet motors,” *Proc. Natl. Acad. Sci. U.S.A.* **107**, 9541–9545 (2010).

[14] A. Sokolov, M. M. Apodaca, B. A. Grzybowski, and I. S. Aranson, “Swimming bacteria power microscopic gears,” *Proc. Natl. Acad. Sci. U.S.A.* **107**, 969–974 (2010).

[15] P. Galajda, J. Keymer, P. Chaikin, and R. Austin, “A wall of funnels concentrates swimming bacteria,” *J. Bacteriol.* **189**, 8704–8707 (2007).

[16] M. B. Wan, C. J. Olson Reichhardt, Z. Nussinov, and C. Reichhardt, “Rectification of swimming bacteria and self-driven particle systems by arrays of asymmetric barriers,” *Phys. Rev. Lett.* **101**, 018102 (2008).

[17] G. Mahmud, C. J. Campbell, K. J. M. Bishop, Y. A. Komarova, O. Chaga, S. Soh, S. Huda, K. Kandere-Grzybowska, and B. A. Grzybowski, “Directing cell motions on micropatterned ratchets,” *Nat. Phys.* **5**, 606–612 (2009).

[18] J. Stenhammar, R. Wittkowski, D. Marenduzzo, and M. E. Cates, “Light-induced self-assembly of active rectification devices,” *Sci. Adv.* **2**, e1501850 (2016).

[19] A. Kaiser, H. H. Wensink, and H. Löwen, “How to capture active particles,” *Phys. Rev. Lett.* **108**, 268307 (2012).

- [20] N. Kumar, R. K. Gupta, H. Soni, S. Ramaswamy, and A. K. Sood, “Trapping and sorting active particles: Motility-induced condensation and smectic defects,” *Phys. Rev. E* **99**, 032605 (2019).
- [21] S. C. Takatori, W. Yan, and J. F. Brady, “Swim pressure: Stress generation in active matter,” *Phys. Rev. Lett.* **113**, 028103 (2014).
- [22] W. Yan and J. F. Brady, “The swim force as a body force,” *Soft Matter* **11**, 6235–6244 (2015).
- [23] A. P. Solon, J. Stenhammar, R. Wittkowski, M. Kardar, Y. Kafri, M. E. Cates, and J. Tailleur, “Pressure and phase equilibria in interacting active brownian spheres,” *Phys. Rev. Lett.* **114**, 198301 (2015).
- [24] A. P. Solon, Y. Fily, A. Baskaran, M. E. Cates, Y. Kafri, M. Kardar, and J. Tailleur, “Pressure is not a state function for generic active fluids,” *Nature Phys.* **11**, 673–678 (2015).
- [25] F. Ginot, I. Theurkauff, D. Levis, C. Ybert, L. Bocquet, L. Berthier, and C. Cottin-Bizonne, “Nonequilibrium equation of state in suspensions of active colloids,” *Phys. Rev. X* **5**, 011004 (2015).
- [26] N. Nikola, A. P. Solon, Y. Kafri, M. Kardar, J. Tailleur, and R. Voituriez, “Active particles with soft and curved walls: Equation of state, ratchets, and instabilities,” *Phys. Rev. Lett.* **117**, 098001 (2016).
- [27] T. Speck and R. L. Jack, “Ideal bulk pressure of active brownian particles,” *Phys. Rev. E* **93**, 062605 (2016).
- [28] G. Junot, G. Briand, R. Ledesma-Alonso, and O. Douchot, “Active versus passive hard disks against a membrane: Mechanical pressure and instability,” *Phys. Rev. Lett.* **119**, 028002 (2017).
- [29] Y. Fily, Y. Kafri, A. P. Solon, J. Tailleur, and A. Turner, “Mechanical pressure and momentum conservation in dry active matter,” *J. Phys. A* **51**, 044003 (2018).
- [30] A. Duzgun and J. V. Selinger, “Active Brownian particles near straight or curved walls: Pressure and boundary layers,” *Phys. Rev. E* **97**, 032606 (2018).
- [31] A. P. Solon, J. Stenhammar, M. E. Cates, Y. Kafri, and J. Tailleur, “Generalized thermodynamics of phase equilibria in scalar active matter,” *Phys. Rev. E* **97**, 020602 (2018).
- [32] L. Angelani, R. Di Leonardo, and G. Ruocco, “Self-starting micromotors in a bacterial bath,” *Phys. Rev. Lett.* **102**, 048104 (2009).
- [33] S. A. Mallory, C. Valeriani, and A. Cacciuto, “Curvature-induced activation of a passive tracer in an active bath,” *Phys. Rev. E* **90**, 032309 (2014).
- [34] R. Ni, M. A. Cohen Stuart, and P. G. Bolhuis, “Tunable long range forces mediated by self-propelled colloidal hard spheres,” *Phys. Rev. Lett.* **114**, 018302 (2015).
- [35] F. Smallenburg and H. Löwen, “Swim pressure on walls with curves and corners,” *Phys. Rev. E* **92**, 032304 (2015).
- [36] L. R. Leite, D. Lucena, F. Q. Potiguar, and W. P. Ferreira, “Depletion forces on circular and elliptical obstacles induced by active matter,” *Phys. Rev. E* **94**, 062602 (2016).
- [37] M. Z. Yamchi and A. Naji, “Effective interactions between inclusions in an active bath,” *J. Chem. Phys.* **147**, 194901 (2017).
- [38] W. Yan and J. F. Brady, “The curved kinetic boundary layer of active matter,” *Soft Matter* **14**, 279–290 (2018).
- [39] Y. Baek, A. P. Solon, X. Xu, N. Nikola, and Y. Kafri, “Generic long-range interactions between passive bodies in an active fluid,” *Phys. Rev. Lett.* **120**, 058002 (2018).
- [40] O. Granek, Y. Baek, Y. Kafri, and A. P. Solon, “Bodies in an interacting active fluid: far-field influence of a single body and interaction between two bodies,” *J. Stat. Mech.: Theory Exp.* **2020**, 063211 (2020).
- [41] D. Saintillan and M. J. Shelley, “Theory of active suspensions,” in *Complex Fluids in Biological Systems*, edited by S. Spagnolie (Springer, New York, NY, 2015) pp. 319–355.
- [42] E. Bertin, M. Droz, and G. Grégoire, “Boltzmann and hydrodynamic description for self-propelled particles,” *Phys. Rev. E* **74**, 022101 (2006).
- [43] W. Yan and J. F. Brady, “The force on a boundary in active matter,” *J. Fluid Mech.* **785**, R1 (2015).
- [44] See Supplemental Material at xxx for details on the simulations, the various analytical calculations, and numerical data for the body shown in Fig. 3.

SUPPLEMENTAL INFORMATION

BROWNIAN DYNAMICS SIMULATIONS

We study an $L \times L$ periodic system of $N = \bar{\rho}L^2$ non-interacting active particles with global number density $\bar{\rho}$. The boomerang-shaped inclusion is composed of equidistant points that lie on a semicircular arc of radius $R = 5$. These points act as force centers and the k th point interacts with the l th active particle at a distance r_{kl} through a shifted Weeks-Chandler-Andersen potential given by

$$u_{kl} = \begin{cases} 4\varepsilon_0 \left[\left(\frac{a}{r_{kl}} \right)^{12} - \left(\frac{a}{r_{kl}} \right)^6 + \frac{1}{4} \right] & \text{if } r_{kl} \leq 2^{1/6}a \\ 0 & \text{otherwise.} \end{cases}$$

Here, a is the potential's length scale and ε_0 is the depth of the energy well. The body shown in Fig. 3 is similarly constructed with points placed on the contour of the shape obtained by displacing two semicircles of radius $R_s = 2.5$ that share their diameters along the diameter. The evolution of the position \mathbf{r}_k and orientation φ_k of the k th active particle is governed by overdamped equations of motion:

$$\dot{\mathbf{r}}_k = v_0 \mathbf{e}_k - \mu_0 \nabla_k U + \sqrt{2D_0} \boldsymbol{\xi}, \quad \dot{\varphi}_k = \sqrt{2D_r} \xi_r \quad (18)$$

where v_0 is the propulsion speed, D_0 is the translational diffusion coefficient, D_r is the rotational diffusion coefficient and $U = \sum_{k,l} u_{kl}$ is the total potential energy due to interactions with the immersed passive body. The mobility $\mu_0 = D_0/(k_B T)$ where $k_B T$ is the thermal energy. The components of $\boldsymbol{\xi}$ and ξ_r are drawn from a uniform distribution over $[-\sqrt{3}, \sqrt{3}]$. We measure lengths in units of a , energy in units of $k_B T$ and time in units of a^2/D_0 . In non-dimensional units, we set $\varepsilon_0 = 100$ and $D_r = 3$.

We integrate Eqs. (18) with time step 10^{-5} . The system is evolved for sufficiently long (at least until $\tau = 100$ in simulation units) so that it reaches steady state following which we measure quantities of interest. All results are ensemble averages over 5 independent runs. For each run, we additionally compute a time average over at least 50 frames with a sampling frequency $\tau' = 1$. The heatmaps shown in Figs. 1, 2, 3 in the main text are obtained by binning the simulation domain with a bin length of a and computing concerned averages within each bin. Spatial derivatives are calculated on the grid using a central difference scheme that respects periodic boundaries. The force on the boomerang \mathbf{F}_1 is calculated by summing over the force on each point that composes it. Identically, the net torque τ_1 is obtained by summing the two-dimensional cross product $\varepsilon_{ij} x_i F_j$ over all points. Here, x_i is the position of the point with respect to the center-of-mass of the body and F_j is the force on the point.

MULTIPOLE EXPANSION

For completeness, we here provide the derivation of the far-field expressions for the current. The analog of the Biot-Savart law in two dimensions for the current yields (for clarity, we write the vector product in three dimensions)

$$\mathbf{j}(\mathbf{r}) = \frac{1}{2\pi} \int d^2 \mathbf{r}' \frac{[\Omega(\mathbf{r}') \mathbf{e}_z] \times (\mathbf{r} - \mathbf{r}')}{|\mathbf{r} - \mathbf{r}'|^2}$$

with curl

$$\begin{aligned} \Omega &\equiv \nabla \times \mathbf{j} = \nabla \times (v_0 \mathbf{p} + \mu_0 \mathbf{F} \rho - D_0 \nabla \rho) \\ &= v_0 \omega + \mu_0 \nabla \times (\mathbf{F} \rho) \end{aligned}$$

and $\omega \equiv \nabla \times \mathbf{p}$. The first two moments are $\tilde{Q} \equiv \int d^2 \mathbf{r} \Omega$ and $\tilde{\mathbf{P}} \equiv \int d^2 \mathbf{r} \mathbf{r} \Omega$, whereby $\tilde{Q} = 0$ due to the same reasons as discussed in the main text for Q .

Employing the Levi-Civita symbol ε_{ij} , we find in cartesian coordinates

$$j_i(\mathbf{r}) = -\frac{1}{2\pi} \varepsilon_{ij} \int d^2 \mathbf{r}' \frac{x_j - x'_j}{|\mathbf{r} - \mathbf{r}'|^2} \Omega(\mathbf{r}'). \quad (19)$$

The Taylor expansion for small \mathbf{r}' reads

$$\frac{x_j - x'_j}{|\mathbf{r} - \mathbf{r}'|^2} \approx \frac{x_j}{r^2} + \left(\frac{\partial}{\partial x_k} \frac{x_j - x'_j}{|\mathbf{r} - \mathbf{r}'|^2} \right)_{\mathbf{r}'=0} x'_k \quad (20)$$

$$= \frac{x_j}{r^2} - \left(\frac{\partial}{\partial x_k} \frac{x_j}{r^2} \right) x'_k. \quad (21)$$

Plugging this expansion back into the current [Eq. (19)] leads to

$$j_i^{\text{ff}} = \frac{1}{2\pi} \varepsilon_{ij} \left(\frac{\partial}{\partial x_k} \frac{x_j}{r^2} \right) \tilde{P}_k = \frac{1}{2\pi} \varepsilon_{ij} \frac{\partial}{\partial x_j} \frac{x_k \tilde{P}_k}{r^2},$$

where in the second step we have exchanged indices using the fact that the expression in brackets is symmetric. Performing the derivative and setting

$$\begin{aligned} m_i &\equiv \varepsilon_{ij} \tilde{P}_j = v_0 \varepsilon_{ij} P_j + \mu_0 \varepsilon_{ij} \int d^2 \mathbf{r} x_j \nabla \times (\mathbf{F} \rho) \\ &= v_0 \varepsilon_{ij} P_j - \mu_0 \varepsilon_{ij} \varepsilon_{jl} \int d^2 \mathbf{r} F_l \rho \end{aligned}$$

leads to the result $\mathbf{m} \equiv v_0 \boldsymbol{\varepsilon} \cdot \mathbf{P} - \mu_0 \mathbf{F}_1$ given in the main text, whereby the boundary of the integral lies within the free region and thus vanishes.

UNBOUNDED SYSTEM: FAR-FIELD REGIME

Dipole moment

The vorticity dipole moment reads

$$\begin{aligned} P_k(A) &= \int_A d^2 \mathbf{r} x_k \varepsilon_{ij} \partial_i p_j \\ &= \oint_{\partial A} d\ell x_k \varepsilon_{ij} n_i p_j - \varepsilon_{kj} \int_A d^2 \mathbf{r} p_j \end{aligned}$$

after integration by parts. Eliminating the polarization in the second term, the dipole moment over a finite area A can be expressed as the contour integral

$$\begin{aligned} P_k(A) &= \oint_{\partial A} d\ell \left[x_k(\mathbf{n} \times \mathbf{p}) - \frac{\mu_0}{v_0} \varepsilon_{kj} n_i \sigma_{ij}^A \right] \\ &= -\frac{1}{2} v_0 \tau_r \oint_{\partial A} d\ell \left[x_k(\mathbf{n} \times \nabla \rho^{\text{ff}}) - \varepsilon_{kj} n_j \delta \rho^{\text{ff}} \right], \end{aligned}$$

where in the second step we have inserted the far-field solution for polarization, $\mathbf{p}^{\text{ff}} = -\frac{1}{2} v_0 \tau_r \nabla \rho^{\text{ff}}$, and active stress, $\mu_0 \boldsymbol{\sigma}_A = -\frac{1}{2} v_0^2 \tau_r \rho \mathbf{1}$ [the polarization gradient does not contribute, cf. Eq. (25)]. Going to a circular boundary with radius r and $\mathbf{n} = \mathbf{e}_r$, we find for an unbounded system

$$\mathbf{P}_{\text{unb}} = -\frac{1}{2} v_0 \tau_r \oint_{\partial A} d\ell \left[\frac{\partial \rho^{\text{ff}}}{\partial \theta} \mathbf{e}_r + \delta \rho^{\text{ff}} \mathbf{e}_\theta \right] = 0$$

using $\boldsymbol{\varepsilon} \cdot \mathbf{e}_r = -\mathbf{e}_\theta$. Both terms cancel since

$$\int_0^{2\pi} d\theta (\cos \theta \mathbf{e}_r + \sin \theta \mathbf{e}_\theta) = 0. \quad (22)$$

Force

The total stress tensor can be written

$$\mu_0 \boldsymbol{\sigma} = -D_{\text{eff}} \rho \mathbf{1} + v_0 \ell^2 (\nabla \mathbf{p})^{ST} \quad (23)$$

with length ℓ and effective diffusion coefficient D_{eff} given in the main text. In the far-field regime, $\mathbf{p}^{\text{ff}} = -\frac{1}{2} v_0 \tau_r \nabla \rho^{\text{ff}}$ with density

$$\rho^{\text{ff}} = \rho_\infty + \frac{1}{D_{\text{eff}}} \frac{\mathbf{m} \cdot \mathbf{r}}{2\pi r^2}.$$

We need the expression

$$\begin{aligned} \mathbf{e}_r \cdot (\nabla \nabla \rho)^{ST} &= \left(2 \frac{\partial^2 \rho}{\partial r^2} - \nabla^2 \rho \right) \mathbf{e}_r \\ &\quad + \frac{2}{r} \left(\frac{\partial^2 \rho}{\partial r \partial \theta} - \frac{1}{r} \frac{\partial \rho}{\partial \theta} \right) \mathbf{e}_\theta. \end{aligned} \quad (24)$$

Inserting ρ^{ff} , we obtain

$$\mathbf{e}_r \cdot (\nabla \nabla \rho^{\text{ff}})^{ST} = \frac{m}{D_{\text{eff}}} \frac{2}{\pi r^3} (\cos \theta \mathbf{e}_r + \sin \theta \mathbf{e}_\theta).$$

Integrating along a circle this contribution vanishes [cf. Eq. (22)] and thus

$$\oint_{\partial A} d\ell \mathbf{e}_r \cdot (\nabla v_0 \mathbf{p})^{ST} = 0 \quad (25)$$

vanishes along a closed circular contour ∂A . The calculation of the force in the far-field regime then reduces to

$$\mu_0 \mathbf{F}_1 = -D_{\text{eff}} \oint_{\partial A} d\ell (\delta \rho^{\text{ff}} - \mathbf{r} \cdot \nabla \rho^{\text{ff}}) \mathbf{e}_r = -\mathbf{m},$$

to which stress and current both contribute $-\mathbf{m}/2$ each.

PERIODIC BOUNDARIES

Density profile for a dipole lattice

Employing periodic boundary conditions is equivalent to periodically replicating the system. The density at \mathbf{r} due to assuming a square lattice of dipoles (each with dipole moment \mathbf{m}) becomes

$$\delta \rho_L^{\text{ff}}(\mathbf{r}) = \sum_n \delta \rho^{\text{ff}}(\mathbf{r} - \mathbf{R}_n) = \frac{1}{D_{\text{eff}}} \sum_n \frac{\mathbf{m} \cdot (\mathbf{r} - \mathbf{R}_n)}{2\pi |\mathbf{r} - \mathbf{R}_n|^2},$$

where n sums over lattice vectors \mathbf{R}_n with $\mathbf{R}_0 = 0$ the origin. We again employ the Taylor expansion Eq. (21) but now for small $|\mathbf{r}| \ll |\mathbf{R}_n|$,

$$\frac{x_i - X_i}{|\mathbf{r} - \mathbf{R}|^2} \approx -\frac{X_i}{\mathbf{R}^2} + \left(\frac{\partial}{\partial X_j} \frac{X_i}{\mathbf{R}^2} \right) x_j,$$

and thus

$$\begin{aligned} \delta \rho_L^{\text{ff}}(\mathbf{r}) &= \delta \rho^{\text{ff}}(\mathbf{r}) + \\ &\quad \frac{1}{2\pi D_{\text{eff}}} \sum_{n \neq 0} \left[\frac{\mathbf{m} \cdot (\mathbf{r} - \mathbf{R}_n)}{\mathbf{R}_n^2} - \mathbf{m} \cdot \frac{2\mathbf{R}_n \mathbf{R}_n}{\mathbf{R}_n^4} \cdot \mathbf{r} \right]. \end{aligned}$$

There are four lattice vectors with the same length $|\mathbf{R}_n| = kL$, two of which sum to zero. Hence,

$$\begin{aligned} \sum_{n \neq 0} \frac{1}{\mathbf{R}_n^2} &= \frac{4}{L^2} \sum_{k=1}^{\infty} \frac{1}{k^2} = \frac{4}{L^2} \frac{\pi^2}{6}, \quad \sum_{n \neq 0} \frac{\mathbf{R}_n}{\mathbf{R}_n^2} = 0, \\ \sum_{n \neq 0} \frac{\mathbf{R}_n \mathbf{R}_n}{\mathbf{R}_n^4} &= \frac{2}{L^2} \mathbf{1} \sum_{k=1}^{\infty} \frac{1}{k^2} = \frac{\pi^2}{3L^2} \mathbf{1} \end{aligned}$$

and the first and third term cancel; to first order of the Taylor expansion there is no correction to the density. Also to second order there is no correction since all terms at this order contain an odd number of lattice vectors.

Vanishing stress contour integral

For the terms involving the current, we need the integrated current

$$J_L = \int_{-\frac{L}{2}}^{+\frac{L}{2}} dx j_y(x, y).$$

With $\nabla \cdot \mathbf{j} = 0$ and $j_x(\pm \frac{L}{2}, y) = 0$ we have

$$\int_{-\frac{L}{2}}^{+\frac{L}{2}} dx \nabla \cdot \mathbf{j} = \int_{-\frac{L}{2}}^{+\frac{L}{2}} dx (\partial_x j_x + \partial_y j_y) = \partial_y J_L = 0,$$

which implies that J_L is uniform throughout the system.

We now investigate the stress Eq. (23) for a line-symmetric body at the origin, cf. Fig. 5. This implies the symmetries

$$\begin{aligned}\rho(-x, y) &= \rho(x, y), \\ p_x(-x, y) &= -p_x(x, y), \\ p_y(-x, y) &= p_y(x, y).\end{aligned}$$

We integrate along the square contour ∂A bounding the finite system with

$$\mathbf{n} \cdot \mu_0 \boldsymbol{\sigma} = -D_{\text{eff}} \rho \mathbf{n} + v_0 \ell^2 [\nabla(\mathbf{n} \cdot \mathbf{p}) - \boldsymbol{\varepsilon} \cdot \nabla(\mathbf{n} \times \mathbf{p})]$$

and piecewise constant normal vector \mathbf{n} . The first contribution from $\rho \mathbf{n}$ vanishes since normal vectors from left/right and top/bottom cancel each other (periodic density).

For the second contribution, let us look at the top boundary at $y = \frac{L}{2}$ with $\mathbf{n} = \mathbf{e}_y$ leading to

$$v_0 \int_{-\frac{L}{2}}^{+\frac{L}{2}} dx [\nabla p_y + \boldsymbol{\varepsilon} \cdot \nabla p_x] = \partial_y \int_{-\frac{L}{2}}^{+\frac{L}{2}} dx v_0 \mathbf{p} = G \mathbf{e}_y,$$

where we used the periodicity of the polarization. In the second step, the x -component is zero because due to the symmetry of the body, the polarization is antisymmetric, $p_x(-x, y) = -p_x(x, y)$. For the y -component, we insert $v_0 p_y = D_0 \partial_y \rho + j_y$ using $\partial_y j_L = 0$ and define

$$G \equiv D_0 \int_{-\frac{L}{2}}^{+\frac{L}{2}} dx \partial_y^2 \rho|_{y=\frac{L}{2}}.$$

The bottom boundary has $\mathbf{n} = -\mathbf{e}_y$ leading to the same G but now with the opposite sign so that these two contributions cancel.

For the right boundary at $x = \frac{L}{2}$ with $\mathbf{n} = \mathbf{e}_x$ we obtain

$$v_0 \int_{-\frac{L}{2}}^{+\frac{L}{2}} dy [\nabla p_x - \boldsymbol{\varepsilon} \cdot \nabla p_y] = \partial_x \int_{-\frac{L}{2}}^{+\frac{L}{2}} dy v_0 \mathbf{p} = 0.$$

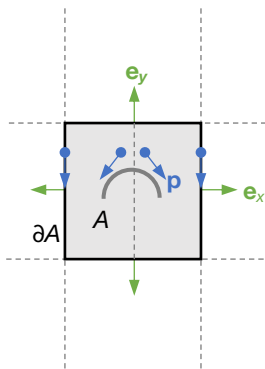


FIG. 5. Sketch of the periodic system with area A and bounded by the square ∂A with normal vectors (green arrows). Sketched are the polarization \mathbf{p} inside and at the left and right boundary (blue arrows).

Now $p_x(\pm \frac{L}{2}, y) = 0$ and the symmetry $p_y(-x, y) = p_y(x, y)$ implies that the derivative $\partial_x p_y$ vanishes. The same holds for the left boundary at $x = -\frac{L}{2}$ and thus

$$\oint_{\partial A} d\ell \mathbf{n} \cdot \boldsymbol{\sigma} = 0.$$

Force, current, and dipole moment

The direct contribution of the current to the force reads

$$\begin{aligned}\oint_{\partial A} d\ell (\mathbf{n} \cdot \mathbf{j}) \mathbf{r} &= \\ \int_{-\frac{L}{2}}^{+\frac{L}{2}} dx [j_y(x, -\frac{L}{2}) \frac{L}{2} + j_y(x, +\frac{L}{2}) \frac{L}{2}] \mathbf{e}_y &= L J_L \mathbf{e}_y\end{aligned}$$

leading to the force $\mathbf{F}_1 = F_L \mathbf{e}_y$ with $F_L = -L J_L / \mu_0$. The x -component of the force vanishes because $j_y(-x) = j_y(x)$ and $j_y(x)x$ is odd.

Using that the total polarization vanishes, the dipole moment can be written

$$\mathbf{P} = \oint_{\partial A} d\ell (\mathbf{n} \times \mathbf{p}) \mathbf{r}.$$

Inserting $v_0 \mathbf{p} = D_0 \nabla \rho + \mathbf{j}$, the density contribution vanishes and the only contribution left is

$$v_0 \mathbf{P} = \int_{-\frac{L}{2}}^{+\frac{L}{2}} dy [j_y(-\frac{L}{2}, y) \frac{L}{2} + j_y(+\frac{L}{2}, y) \frac{L}{2}] \mathbf{e}_x = L^2 j_0 \mathbf{e}_x.$$

Since on the boundary $j_x = 0$, divergence-free $\partial_y j_y = 0$ requires $j_y(\pm \frac{L}{2}, y) = j_0$ to be constant.

Scaling of current

The current through the system is generated by the density difference of the accumulated active particles at the body. Eq. (10) in the main text suggests

$$J_L = -D_{\text{eff}} \bar{\rho} \alpha_L$$

with dimensionless gradient $\alpha_L > 0$ across the boomerang with radius R . For small L , increasing L adds streamlines connecting through the periodic boundaries and increases the current, $\alpha_L \sim L/\ell$, with decay length ℓ governing the current. For large L , we expect $\alpha_L \sim R/L$ to be self-similar. Assuming that α_L depends on the system parameters only through the dimensionless combination $L/\sqrt{\ell R}$, the current through the cross section can be written

$$J_L = -\bar{\rho} D_{\text{eff}} \frac{L}{\ell} f(L/\sqrt{\ell R}) \sim \bar{\rho} D_{\text{eff}} \begin{cases} L/\ell & (L \ll L^*) \\ R/L & (L \gg L^*) \end{cases}$$

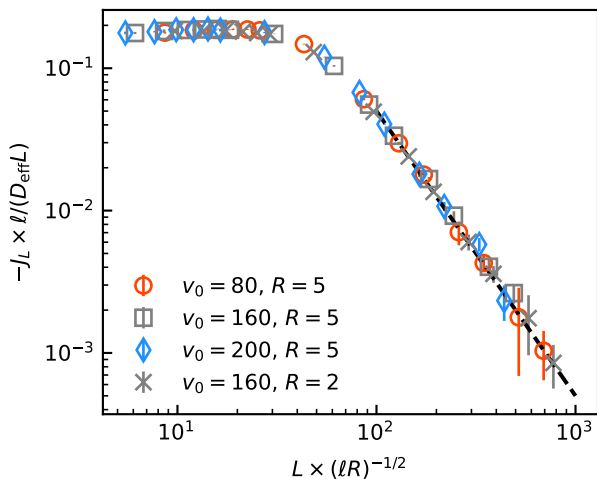


FIG. 6. Integrated current J_L for the boomerang as a function of the scaled system size $L/\sqrt{\ell R}$ for several speeds v_0 and two radii R . The dashed line shows $f \sim x^{-2}$.

with scaling function $f(x)$, which is constant for small x and decays as $f(x) \sim x^{-2}$ for large x . In Fig. 6, we demonstrate that the numerical current as a function of $L/\sqrt{\ell R}$ indeed collapses onto a single curve $f(x)$ for several speeds v_0 and sizes R of the obstacle. The crossover length L^* scales as $L^* = x^* \sqrt{\ell R}$ with $x^* \simeq 50$.

Note that for large speeds $v_0 \gg 4\sqrt{D_0/\tau_r}$, we have

$$\ell \approx \frac{v_0 \tau_r}{4}, \quad D_{\text{eff}} \approx \frac{1}{2} v_0^2 \tau_r,$$

whereas $\xi \approx \sqrt{D_0 \tau_r / 8}$ becomes independent of the speed. For the force, we thus find

$$\mu_0 F_L = -L J_L \sim \bar{\rho} \begin{cases} v_0 L^2 & (L \ll L^*) \\ v_0^2 \tau_r R & (L \gg L^*) \end{cases}$$

in agreement with Figure 2(b) in the main text. This scaling is different from the one reported by Mallory *et al.* [PRE **90**, 032309 (2014)] for a bath of underdamped self-propelled particles.

TORQUE

Unbounded system

Inserting the force-balance, the torque can be written as the integral

$$\tau_1 = \int_A d^2 \mathbf{r} \varepsilon_{ij} x_i [\partial_k \sigma_{kj} - j_j / \mu_0].$$

The first term can be manipulated into

$$\begin{aligned} \varepsilon_{ij} x_i \partial_k \sigma_{kj} &= \varepsilon_{ij} [\partial_k (x_i \sigma_{kj}) - \sigma_{ij}] \\ &= \varepsilon_{ij} \partial_k (x_i \sigma_{kj}) \end{aligned}$$

using that the stress is symmetric, $\sigma_{ij} = \sigma_{ji}$. Exploiting the divergence theorem, we obtain

$$\tau_1 = \oint_{\partial A} dl \varepsilon_{ij} x_i n_k \sigma_{kj} - \frac{1}{\mu_0} \int_A d^2 \mathbf{r} \mathbf{r} \times \mathbf{j}.$$

The next step is to insert the stress choosing a circular boundary ∂A with radius r and normal vector $\mathbf{n} = \mathbf{e}_r$. It is easy to see that the isotropic part cancels since on the boundary $\mathbf{r} \times \mathbf{n} = 0$. For the second derivatives of the density $\rho(r, \theta)$ we employ Eq. (24). Taking the vector product $\mathbf{r} \times (\varepsilon_{ij} x_i)$ only the second term survives with $\mathbf{r} \times \mathbf{e}_\theta = r$. However, integrating this term along a closed circular boundary yields zero since the density necessarily is periodic with respect to θ ,

$$\int_0^{2\pi} d\theta \frac{\partial \rho}{\partial \theta} = 0.$$

This leaves us with a torque [using $\varepsilon_{ij} x_i n_k \partial_k j_j = n_k \partial_k (\varepsilon_{ij} x_i j_j) - \varepsilon_{ij} n_i j_j$]

$$\begin{aligned} \tau_1 &= \frac{\ell^2}{\mu_0} \oint_{\partial A} dl [\mathbf{n} \cdot \nabla (\mathbf{r} \times \mathbf{j}) + (\mathbf{r} \times \nabla) \mathbf{n} \cdot \mathbf{j} - \mathbf{n} \times \mathbf{j}] \\ &\quad - \frac{1}{\mu_0} \int_A d^2 \mathbf{r} \mathbf{r} \times \mathbf{j}. \end{aligned}$$

The second term involves $\partial_\theta j_r$ and vanishes after integration. Sticking with the circular boundary, the other three terms involve the integral

$$\int_0^{2\pi} d\theta \mathbf{r} \times \mathbf{j} = \int_0^{2\pi} d\theta r j_\theta = v_0 Q$$

and thus $\tau_1 \propto v_0 Q$.

Periodic system

Figure 7 shows numerical results for the torque exerted on the body discussed in the main page. As for translational forces, we find that initially $\tau_1 \sim v_0 L^2$ in finite systems with periodic boundaries.

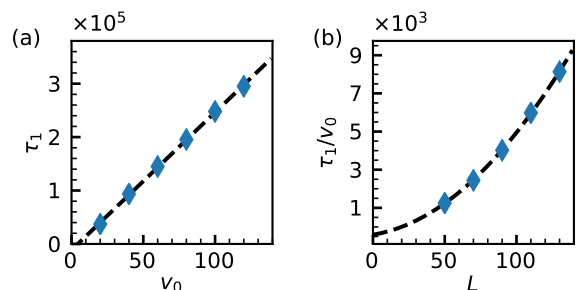


FIG. 7. Numerical results for the torque on the C_2 -symmetric body shown in Fig. 3 of the main text. Torque τ_1 (a) as a function of propulsion speed v_0 (the dashed line is a linear fit) and (b) as a function of system size L (the dashed line is a quadratic fit).